

Plasma density optimisation of laser-wakefield acceleration for high-brightness bremsstrahlung emission applied to advanced manufacturing imaging.

*Contact: chris.baird@stfc.ac.uk

C. D. Baird*, C. Armstrong, D. R. Rusby,
D. R. Symes, C. Thornton, C. M. Brenner
*Central Laser Facility, STFC Rutherford Appleton
Laboratory, Didcot OX11 0QX, UK*

S. Cipiccia
*Diamond Light Source, STFC Rutherford Appleton
Laboratory, Didcot OX11 0QX, UK*

C. I. D. Underwood, C. D. Murphy
*York Plasma Institute, Department of Physics,
University of York, York YO10 5DD, UK*

Abstract

Laser-wakefield acceleration of electrons generates high-energy beams that when propagated through solid materials will stimulate bremsstrahlung X-ray emission that has both small ($< 50 \mu\text{m}$) source size and high energy ($> 1 \text{ MeV}$) for achieving high resolution penetrative radiography. Laser-driven X-ray imaging requires bright beams for high signal-to-noise acquisition and therefore high-quality imaging. X-ray emission is dependent on the electron beam charge and spectral distribution, therefore mechanisms for optimising and tuning the electron beam properties are advantageous for development of this source for applications. Here we report on X-ray emission optimised for different material properties by varying the gas pressure of the wakefield accelerator. Experimental results are presented of LWFA electron beam charge and X-ray emission after the beam is incident on a range of converter materials to produce bremsstrahlung. The X-rays were then used to image a number of high-density, industrially-relevant samples with sub-millimetre internal features to demonstrate the capability of this new X-ray technology.

1 Introduction

Modern high-power, short-pulse lasers have been used in recent years to develop compact particle acceleration schemes. Laser wakefield acceleration (LWFA) uses laser-driven plasma waves to trap and accelerate electrons. Significant advances have been made since LWFA was originally conceived by Tajima and Dawson [1], with experimental results demonstrating high-quality electron beams [2–4] with energies in the multi-GeV range [5–7].

One of the many applications of such compact electron sources is the production of high-brightness, ultra-short X-ray sources. Transverse oscillations of the electrons

O. J. Finlay
*The Cockcroft Institute Daresbury Laboratory, Sci-Tech
Daresbury, Daresbury WA4 4AD, UK*

M. J. V. Streeter, J.-N. Gruse, Z. Najmudin
*The John Adams Institute for Accelerator Science, Imperial
College London, London SW7 2AZ, UK*

as they are accelerated generate betatron radiation [8] which, due to its small source size and high-spatial coherence, is ideal for phase-contrast imaging [9–11]. Colliding the LWFA electrons with a laser pulse, i.e. Compton backscattering, is an effective way to produce MeV-scale, monoenergetic X-rays [12, 13]. For an in-depth review of the recent developments in LWFA light sources, see Corde *et al.* (2013) [14] and Albert *et al.* (2016) [15].

Compact X-ray sources for imaging have also been demonstrated using bremsstrahlung [16–19]. Electrons incident on a high-Z material produce a broad, synchrotron-like spectrum with a tail extending up to the peak electron energy. In situations where high photon energy is required for penetration of dense materials, and where the complexity of the setup must be minimised, bremsstrahlung sources have a distinct advantage over both betatron and Compton sources. One such situation is that of non-destructive testing (NDT) in industrial settings, where the materials in question are often composed of high-density metals such as steel or nickel, and may contain small internal features.

The current industry-standard approach to NDT is to use a linear accelerator to produce electrons, which are then converted to bremsstrahlung by conversion through high-Z material. However, commercial linac sources are often limited to millimetre-scale source sizes [20], or sub-MeV energy [21]. Laser-driven bremsstrahlung sources, on the other hand, can readily achieve multi-MeV energies with high flux and micron-scale source size, capable of penetrating even the densest materials.

In this report we present the results of a recent experiment on the Gemini laser, where we demonstrate imaging of industrial materials using a LWFA bremsstrahlung source. Additionally we show that the source can be tuned to accommodate a range of material properties.

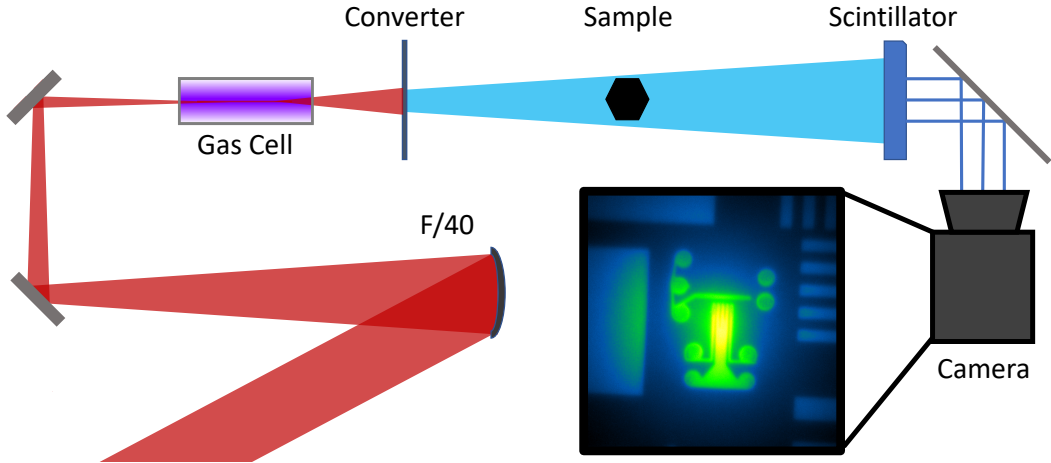


Figure 1: Schematic of the experimental setup. Using an F/40 parabolic mirror, the laser is focussed into a 15mm gas cell. Electrons produced by the laser interact with a converter target, producing X-rays and projecting an image of the sample onto the scintillator.

2 Experimental Setup

To generate the electron beam, we focussed the South beam of the Gemini laser into a 15mm gas cell with an $f/40$ parabolic mirror, delivering 6J of energy in 50 fs. The size of the focal spot was measured to be $50\ \mu\text{m} \times 40\ \mu\text{m}$, giving a peak intensity of $2.9 \times 10^{18}\ \text{W cm}^{-2}$ ($a_0 \simeq 1.2$). After passing through the gas cell, the laser pulse was redirected to a beam dump by a strip of polyimide tape. The accelerated electron bunch was then propagated through a converter material mounted 50mm behind the gas cell, after which it was dispersed by a magnetic spectrometer.

By varying the backing pressure of the gas cell, the properties of the electron bunch can be changed. An increase in pressure, i.e. electron density, typically results in an increase in the total accelerated charge and a decrease in the maximum electron energy, enabling tuning of the bremsstrahlung radiation from the converter.

A range of samples were mounted in one of three positions of varying distance from the source, allowing the field of view and magnification to be adjusted to the sample dimensions. Two sample positions were inside the vacuum chamber ($M=10$ and $M=2.5$), and the other outside ($M=1.6$). The attenuation of X-rays leaving the chamber was minimised by using a thin polyimide window. X-rays from each converter were first characterised using an array of caesium iodide crystals to measure the beam divergence and energy spectrum. This diagnostic was then replaced with an imaging detector comprising a scintillator imaged with an optical CCD camera.

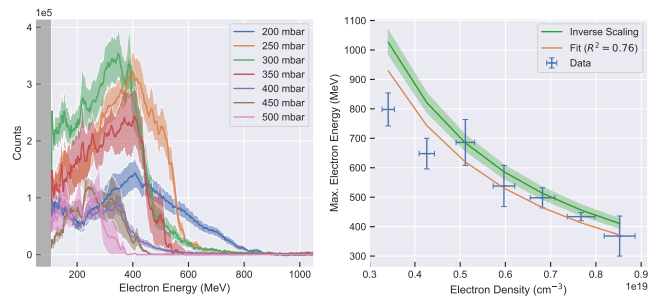


Figure 2: Left: Comparison of electron spectra as a function of backing pressure on the gas cell. Each line shows the mean of all shots taken at a particular pressure setting. Right: Maximum electron energy as a function of backing pressure.

3 Source Characterisation

3.1 Electron Beam

The mean electron spectrum for each backing pressure is shown in Fig. 2. From these data, it can be seen that the accelerated charge was highest for backing pressures of 250 and 300 mbar. Figure 3 illustrates this more clearly, showing that the total charge was optimised at an electron density of $\simeq 4.4 \times 10^{18}\ \text{cm}^{-3}$.

An increase in backing pressure results in a reduction in the maximum electron energy due to a decrease in the dephasing length. Varying the backing pressure between 200 and 500mbar reduced the maximum energy from $798 \pm 56\ \text{MeV}$ to $368 \pm 68\ \text{MeV}$. The maximum electron energy for each pressure setting is shown in Fig. 2 (right). A line corresponding to the inverse scaling estimate for maximum energy gain due to dephasing, $w_{max} = 2m_e c^2 n_c / n_e$ [22] is also shown.

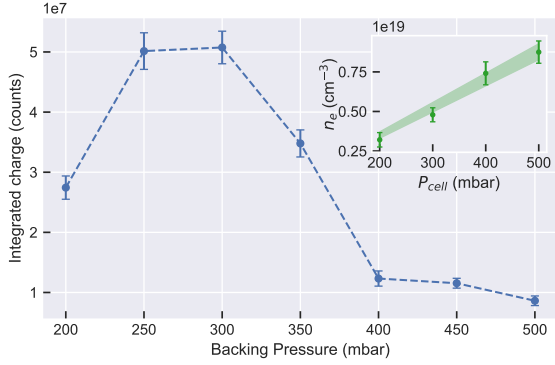


Figure 3: Total charge (uncalibrated) as a function of pressure. Each point is the integrated counts for the corresponding spectrum in Fig. 2 (left). The peak charge occurs at 300 mbar. The inset shows the measured electron density as a function of the backing pressure.

3.2 X-Ray Beam

Initial characterisation of the X-ray beam was conducted using an array of CsI crystals, which were oriented perpendicular to the beam propagation direction. This allows us to observe the attenuation of the beam by each successive layer of crystals. By measuring the width of the signal in the first row of crystals, we can infer the divergence angle of the beam. Figure 4 shows an example of the signal on the detector.

It can be seen from Fig. 5 (top) that the variation in measured X-ray signal due to a change in backing pressure approximately follows that of the total electron charge (Fig. 3). Specifically, the peak of the signal occurs at the same pressure as the peak electron charge. This suggests that the electron charge produced below the minimum range of the spectrometer (104 MeV), i.e. that most efficiently converted to X-rays, is relatively low.

By increasing the backing pressure from 200 mbar to 400 mbar, the divergence angle of the X-rays (Fig. 5 (bottom)) increases. As the opening angle of the bremsstrahlung beam scales with $1/\gamma_e$, this is consistent with the variation in measured electron energy with pressure.

After characterising the X-ray beam using the CsI array, the detector was changed to a LYSO crystal which was imaged on-axis. A typical beam profile in the LYSO configuration is shown in Fig. 4. This arrangement allowed us to use the X-ray beam as a backlighter for imaging samples.

3.3 Imaging Quality

To quantify the imaging quality of the source, we illuminated a tungsten resolution grid with the X-ray beam and captured the resulting projection using image plate and also with an 8mm thick LYSO crystal. Measurements of 200 μm features are shown in Fig. 6. The contrast of the features was found to be $67 \pm 4\%$ with the

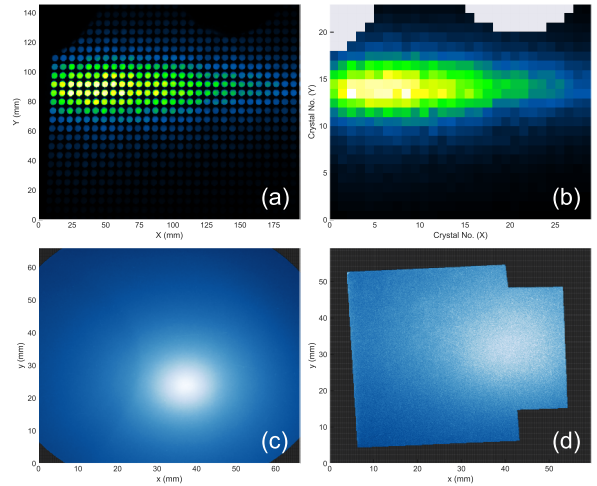


Figure 4: X-ray signal images. (a) Raw CsI signal; (b) Crystal values extracted from signal; (c) 8 mm thick LYSO crystal ($r = 40$ mm); (d) 2 mm thick LYSO crystal (50 mm \times 50 mm)

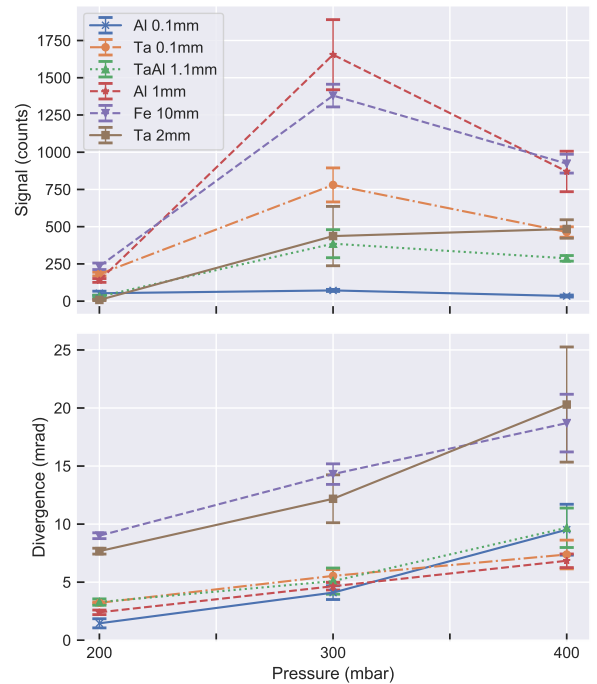


Figure 5: Top: Effect of backing pressure on signal amplitude observed by CsI detector for 6 converter types. The converter labelled ‘TaAl 1.1mm’ is a layered target comprised of 0.1mm Ta and 1mm Al. Bottom: Divergence angle for each converter.

image plate, but the LYSO caused significant blurring, reducing the contrast to around 2%. The scintillator crystal was then replaced with 2mm thick LYSO for comparison. With the thinner crystal, we were able to obtain a contrast of just over 20% on 150 μm features on the resolution grid, as shown in Fig. 7.

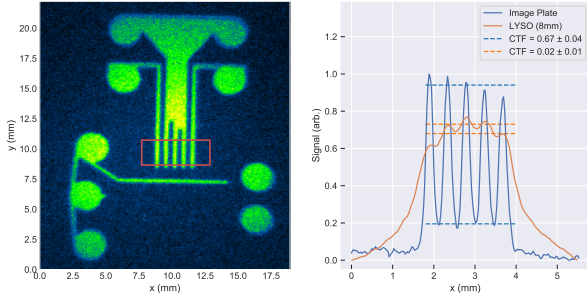


Figure 6: Left: Image plate scan of resolution grid. Features in the red box are 200 μm . Right: Contrast of 200 μm features as measured with image plate, and 8mm thick LYSO. The scintillator material causes significant blurring due to its thickness.

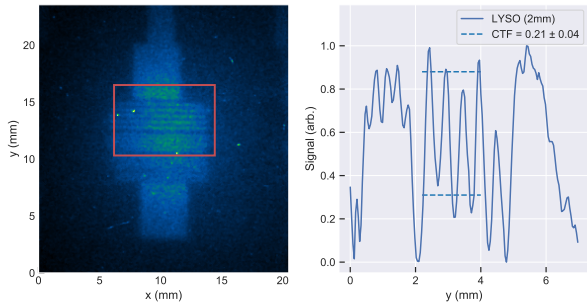


Figure 7: Left: Image of thin foils captured by 2mm LYSO. Right: A contrast of 0.21 ± 0.04 was measured for the highlighted region, which contains foils 150 μm thick.

Although a direct measurement of the source size was not obtained, the significant difference in contrast between the detector types (image plate, 8mm and 2mm LYSO) demonstrates that the imaging quality in our setup is limited by the detector itself, and not by the source size.

4 Monte Carlo Simulations

The spectral profile of the X-rays was inferred by simulating the interaction of the electrons with the converter targets using GEANT4.

An ensemble of 10^5 electrons was collided with each converter. The emitted photons were counted at a distance of 25mm behind the target, then processed into 2MeV bins. Because the electrons cannot be measured after interaction with the converter due to scattering and

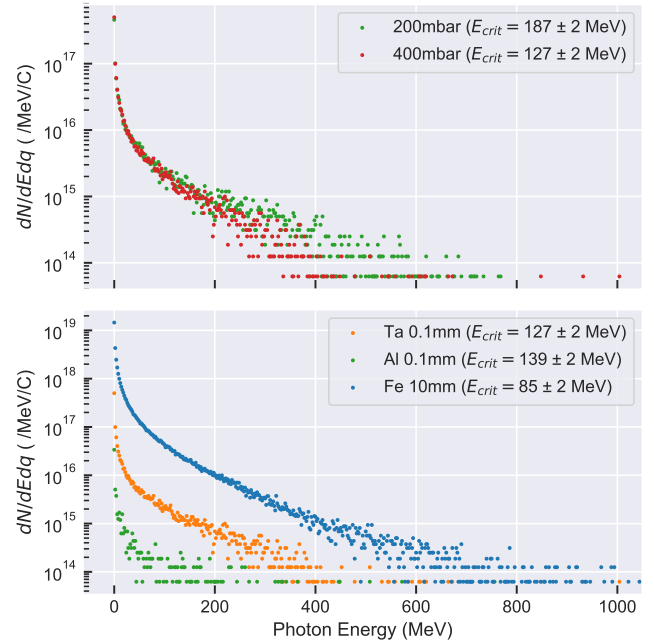


Figure 8: Top: Photon spectra for 0.1mm Ta at 200 mbar (green) and 400 mbar (red). A decrease in pressure leads to an increase in critical energy; Bottom: Photon spectra for 3 different converters at 400 mbar backing pressure. A range of critical energy values can be obtained by choice of converter material.

absorption, the mean electron spectra measured without the converter in place were used as the input.

The spectral composition of the bremsstrahlung beam can be characterised by the ‘critical energy’, E_{crit} , defined as the energy above which 50% of the total photon energy is radiated. A larger value of E_{crit} is indicative of a higher penetrating power.

Figure 8 shows that increasing the backing pressure from 200 to 400 mbar, i.e. decreasing the mean electron energy, corresponds to a decrease in the characteristic energy of the X-rays. This indicates that we are able to tune the spectral characteristics of the X-ray beam for different material properties, simply by changing the backing pressure. Figure 8 (bottom) shows the change in spectral shape for different converters at the same pressure (400 mbar).

5 Sample Imaging

To test the imaging capability of the source, we used a variety of samples provided by industrial collaborators. Figure 9 (left) shows one example, an additively-manufactured star composed of the nickel alloy Inconel which is around 5cm thick in the longitudinal direction. This was placed outside the target chamber ($M=1.6$), and imaged using bremsstrahlung from a 2mm tantalum converter.

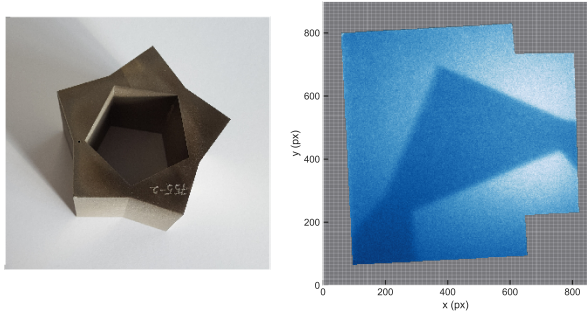


Figure 9: Left: Photograph of Inconel star object. Right: 2 mm LYSO image of star. The X-ray beam profile is just visible inside the dark region, showing the penetration capability of the source.

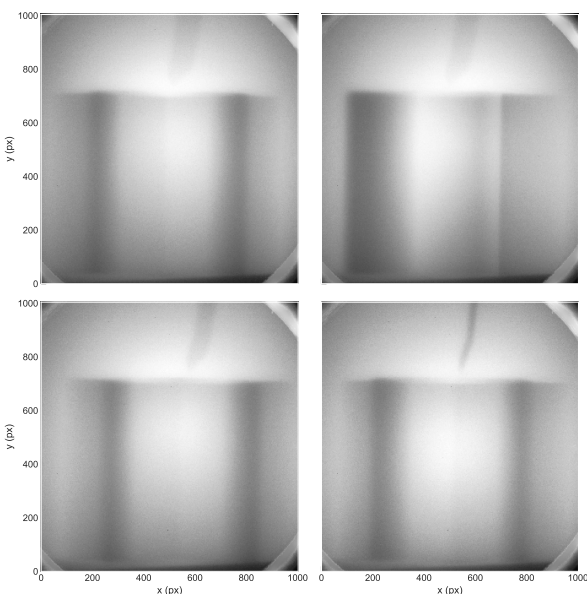


Figure 10: 8 mm LYSO images of nickel alloy star at various angular orientations, showing potential for tomographic reconstruction.

Figure 9 (right) shows the star imaged top-down with a 2 mm LYSO crystal, where the profile of the X-ray beam can be seen in the attenuated region, demonstrating the penetration capability. Figure 10 shows side projections of the star, imaged with an 8 mm LYSO crystal. The acquisition of multiple projections demonstrates the potential to use the laser-driven source for tomographic reconstruction of industrial objects.

6 Summary

Using laser-wakefield accelerated electrons and metallic converter materials, we have produced a bremsstrahlung X-ray source capable of imaging of high-density, industrially relevant materials with a resolution of 150 μm , currently limited by the detector. This is significantly

better than the industry-standard of ~ 1 mm. By varying the backing pressure of the gas target or the converter type, we are able to control the brightness, divergence, and the characteristic temperature of the X-ray beam.

7 Acknowledgements

The authors thank the staff at the Central Laser Facility and acknowledge funding from STFC (grant numbers ST/P002056/1 and ST/P002021/1). We thank the Manufacturing Technology Centre for providing the Inconel sample and acknowledge fruitful discussions with Nick Brierley.

References

- [1] T. Tajima and J. M. Dawson. Laser electron accelerator. *Physical Review Letters*, 43(4):267–270, 1979. ISSN 00319007. doi: 10.1103/PhysRevLett.43.267.
- [2] S. P. D. Mangles, C. D. Murphy, Z. Najmudin, A. G. R. Thomas, J. L. Collier, A. E. Dangor, E. J. Divall, P. S. Foster, J. G. Gallacher, C. J. Hooker, D. A. Jaroszynski, A. J. Langley, W. B. Mori, P. A. Norreys, F. S. Tsung, R. Viskup, B. R. Walton, and K. Krushelnick. Monoenergetic beams of relativistic electrons from intense laser-plasma interactions. *Nature*, 431(7008):535–538, 2004. ISSN 0028-0836. doi: 10.1038/nature02939.
- [3] C. G. R. Geddes, C. S. Tóth, J. Van Tilborg, E. Esarey, C. B. Schroeder, D. Bruhwiler, C. Nieter, J. Cary, and W. P. Leemans. High-quality electron beams from a laser wakefield accelerator using plasma-channel guiding. *Nature*, 431(7008):538–541, 2004. ISSN 0028-0836. doi: 10.1038/nature02900.
- [4] J. Faure, Y. Glinec, A. Pukhov, S. Kiselev, S. Gordienko, E. Lefebvre, J-P. Rousseau, F. Burgy, and V. Malka. A laserplasma accelerator producing monoenergetic electron beams. *Nature*, 431(September):541–544, 2004. doi: 10.1038/nature02900.1.
- [5] W. P. Leemans, B. Nagler, A. J. Gonsalves, Cs Tóth, K. Nakamura, C. G.R. Geddes, E. Esarey, C. B. Schroeder, and S. M. Hooker. GeV electron beams from a centimetre-scale accelerator. *Nature Physics*, 2(10):696–699, 2006. ISSN 17452473. doi: 10.1038/nphys418.
- [6] Hyung Taek Kim, Ki Hong Pae, Hyuk Jin Cha, I. Jong Kim, Tae Jun Yu, Jae Hee Sung, Seong Ku Lee, Tae Moon Jeong, and Jongmin Lee. Enhancement of electron energy to the multi-gev regime by a dual-stage laser-wakefield accelerator pumped by petawatt laser pulses. *Physical Review Letters*, 111(16):1–5, 2013. ISSN 00319007. doi: 10.1103/PhysRevLett.111.165002.
- [7] Xiaoming Wang, Rafal Zgadzaj, Neil Fazel, Zhengyan Li, S. A. Yi, Xi Zhang, Watson Henderson, Y. Y. Chang, R. Korzekwa, H. E. Tsai, C. H. Pai, H. Quevedo, G. Dyer, E. Gaul, M. Martinez, A. C. Bernstein, T. Borger, M. Spinks, M. Donovan, V. Khudik, G. Shvets, T. Ditmire, and M. C. Downer. Quasi-monoenergetic laser-plasma acceleration of electrons to 2 GeV. *Nature Communications*, 4(May):1988, 2013. ISSN 20411723. doi: 10.1038/ncomms2988. URL <http://www.nature.com/ncomms/2013/130611/ncomms2988/full/ncomms2988.html%5Cnhttp://www.nature.com/doi/finder/10.1038/ncomms2988>.

- [8] Antoine Rousse, Kim Ta Phuoc, Rahul Shah, Alexander Pukhov, Eric Lefebvre, Victor Malka, Sergey Kiselev, Frédéric Burgy, Jean Philippe Rousseau, Donald Umstadter, and Danièle Hulin. Production of a keV X-ray beam from synchrotron radiation in relativistic laser-plasma interaction. *Physical Review Letters*, 93(13):1–4, 2004. ISSN 00319007. doi: 10.1103/PhysRevLett.93.135005.
- [9] S. Fourmaux, S. Corde, K. Ta Phuoc, P. Lassonde, G. Lebrun, S. Payeur, F. Martin, S. Sebban, V. Malka, A. Rousse, and J. C. Kieffer. Single shot phase contrast imaging using laser-produced Betatron x-ray beams. *Optics letters*, 36(13):2426–8, 2011. ISSN 1539-4794. doi: 10.1364/OL.36.002426. URL <http://www.osapublishing.org/viewmedia.cfm?uri=ol-36-13-2426&seq=0&html=true>.
- [10] S. Kneip, C. McGuffey, F. Dollar, M. S. Bloom, V. Chvykov, G. Kalintchenko, K. Krushelnick, A. Maksimchuk, S. P.D. Mangles, T. Matsuoka, Z. Najmudin, C. A.J. Palmer, J. Schreiber, W. Schumaker, A. G.R. Thomas, and V. Yanovsky. X-ray phase contrast imaging of biological specimens with femtosecond pulses of betatron radiation from a compact laser plasma wakefield accelerator. *Applied Physics Letters*, 99(9):1–4, 2011. ISSN 00036951. doi: 10.1063/1.3627216.
- [11] A. Döpp, L. Hehn, J. Goetzfried, J. Wenz, M. Gilljohann, H. Ding, S. Schindler, F. Pfeiffer, and S. Karsch. Quick X-ray microtomography using a laser-driven betatron source. *Optica*, 5(2):5–9, 2018. URL <http://arxiv.org/abs/1712.08761>.
- [12] S. Chen, N. D. Powers, I. Ghebregziabher, C. M. Maharjan, C. Liu, G. Golovin, S. Banerjee, J. Zhang, N. Cunningham, A. Moorti, S. Clarke, S. Pozzi, and D. P. Umstadter. MeV-Energy X Rays from Inverse Compton Scattering with Laser-Wakefield Accelerated Electrons. *Physical Review Letters*, 110(15):155003, 2013. doi: 10.1103/PhysRevLett.110.155003.
- [13] N. D. Powers, I. Ghebregziabher, G. Golovin, C. Liu, S. Chen, S. Banerjee, J. Zhang, and D. P. Umstadter. Quasi-monoenergetic and tunable X-rays from a laser-driven Compton light source. *Nature Photonics*, 8(1):28–31, 2013. ISSN 1749-4885. doi: 10.1038/nphoton.2013.314. URL <http://dx.doi.org/10.1038/nphoton.2013.314>.
- [14] S. Corde, K. Ta Phuoc, G. Lambert, R. Fitour, V. Malka, A. Rousse, A. Beck, and E. Lefebvre. Femtosecond x rays from laser-plasma accelerators. *Reviews of Modern Physics*, 85(1), 2013. ISSN 00346861. doi: 10.1103/RevModPhys.85.1.
- [15] Félicie Albert and Alec G R Thomas. Applications of laser wakefield accelerator-based light sources. *Plasma Physics and Controlled Fusion*, 58:103001, 2016. doi: 10.1088/0741-3335/58/10/103001.
- [16] R. D. Edwards, M. A. Sinclair, T. J. Goldsack, K. Krushelnick, F. N. Beg, E. L. Clark, A. E. Dangor, Z. Najmudin, M. Tatarakis, B. Walton, M. Zepf, K. W. D. Ledingham, I. Spencer, P. A. Norreys, R. J. Clarke, R. Kodama, Y. Toyama, and M. Tampo. Characterization of a gamma-ray source based on a laser-plasma accelerator with applications to radiography. *Applied Physics Letters*, 80(12):2129–2131, 2002. ISSN 0003-6951. doi: 10.1063/1.1464221.
- [17] Y Glinec, J Faure, L Le Dain, S Darbon, T Hosokai, J J Santos, E Lefebvre, J P Rousseau, F Burgy, B. Mercier, and V. Malka. High-Resolution γ -Ray Radiography Produced by a Laser-Plasma Driven Electron Source. *Phys. Rev. Lett.*, 94:025003, 2005. doi: 10.1103/PhysRevLett.94.025003.
- [18] A Döpp, E Guillaume, C Thauray, A Lifschitz, F Sylla, J-P Goddet, A Tafzi, G Iaquanello, T Lefrou, P Rousseau, E Conejero, C Ruiz, K Ta Phuoc, and V Malka. A bremsstrahlung gamma-ray source based on stable ionization injection of electrons into a laser wakefield accelerator. *Nuclear Inst. and Methods in Physics Research, A*, 830:515–519, 2016. ISSN 0168-9002. doi: 10.1016/j.nima.2016.01.086. URL <http://dx.doi.org/10.1016/j.nima.2016.01.086>.
- [19] K. Dong, T. Zhang, M. Yu, Y. Wu, B. Zhu, F. Tan, S. Wang, Y. Yan, J. Yang, Y. Yang, F. Lu, G. Li, W. Fan, W. Hong, Z. Zhao, W. Zhou, L. Cao, and Y. Gu. Micro-spot gamma-ray generation based on laser wakefield acceleration. *Journal of Applied Physics*, 123(July 2017):243301, 2018. doi: 10.1063/1.4997142.
- [20] Varex Imaging. Linatron Linear Accelerators, 2019. URL <https://www.vareximaging.com/products/security-industrial/linear-accelerators>.
- [21] A. Ramsey and C. Rudolf. A 750kV microfocus X-ray source with a 30 μm spot size, 2019. URL https://www.ndt.net/events/ECNDT2014/app/content/Slides/439_Ramsey.pdf.
- [22] E. Esarey, C. B. Schroeder, and W. P. Leemans. Physics of laser-driven plasma-based electron accelerators. *Reviews of Modern Physics*, 81(3):1229–1285, 2009. ISSN 00346861. doi: 10.1103/RevModPhys.81.1229.